Available online at www.sciencedirect.com
ScienceDirect
Journal of Solid State Chemistry 180 (2007) 3211–3217
JOURNAL OF SOLID STATE CHEMISTRY
www.elsevier.com/locate/jssc

Magnetic and thermoelectric properties of layered $Li_xNa_yCoO_2$

J.W.G. Bos*, J.T. Hertz, E. Morosan, R.J. Cava

Department of Chemistry, Princeton University, Princeton, New Jersey 08544, USA

Received 15 June 2007; received in revised form 1 September 2007; accepted 3 September 2007
Available online 8 September 2007

Abstract

The magnetic, thermoelectric, and structural properties of $Li_xNa_yCoO_2$, prepared by intercalation and deintercalation chemistry from the thermodynamically stable phase $Li_{0.41}Na_{0.31}CoO_2$, which has an alternating Li/Na sequence along the *c*-axis, are reported. For the high Li-Na content phases $Li_{0.41}Na_{0.31}CoO_2$ and $Li_{0.40}Na_{0.43}CoO_2$, a sudden increase in susceptibility is seen below 50 K, whereas for $Li_{0.21}Na_{0.14}CoO_2$ an antiferromagnetic-like transition is seen at 10 K, in spite of a change from dominantly antiferromagnetic to dominantly ferromagnetic interactions with decreasing alkali content. The Curie constant decreases linearly with decreasing alkali content, at the same time the temperature-independent contribution to the susceptibility increases, indicating that as the Co becomes more oxidized the electronic states become more delocalized. Consistent with this observation, the low alkali containing phases have metallic-like resistivities. The 300 K thermopowers fall between 30 μV/K ($x+y=0.31$) and 150 μV/K ($x+y=0.83$).
Published by Elsevier Inc.

Keywords: Lithium sodium cobalt oxide; Layered cobalt oxide; Thermoelectric; Magnetism

1. Introduction

The study of layered A_xCoO_2 cobaltates (A = Li or Na) is of interest from the viewpoint of both basic science and industrial applications. Li_xCoO_2 is used in Li-ion batteries [1] while Na_xCoO_2 shows a wide variety of electronic states [2], including high thermopower [3,4] and superconductivity when water is intercalated [5]. The compounds are based on triangular CoO_2 layers built from CoO_6 octahedra sharing edges, alternating with layers of alkali ions. A single thermodynamically stable $LiCoO_2$ phase exists [1,6] while for Na_xCoO_2 three thermodynamically stable phases can be obtained [7–9]. These phases are distinguished by the Na content, number of CoO_2 sheets per unit cell (1, 2 or 3), and by the coordination of the alkali ion (trigonal prismatic or octahedral). By changing the alkali content by chemie douce or electrochemical methods, the electronic properties of the family can be tuned.

Na_xCoO_2 is found in both 2- and 3-layer derived series. Both show similar electronic properties as a function of x in spite of differences in the crystal structures due to layer stacking [8,9]. This suggests that the physical properties are dominated by charge transport within the CoO_2 layers, with the band filling controlled via the Na content. For Li_xCoO_2, only a 3-layer derived series exists. There are clear similarities between the Na and Li series: an insulator to metal transition is observed on decreasing x, and at $x=0.5$ an A^+/vacancy ordering is reported [2,10]. One notable difference is the impossibility (so far) of making a suitably water intercalated, superconducting $Li_{0.3}CoO_2$: yH_2O phase [11]. Here we report an investigation into a related layered cobaltate that contains distinct layers of Li and Na between CoO_2 planes.

The synthesis and structural characterization of a thermodynamically stable $Li_xNa_yCoO_2$ phase was first reported by Balsys and Davis [12]. Their sample had composition $Li_{0.43(2)}Na_{0.36(2)}CoO_{1.96(6)}$ and was found to crystallize in space group $P6_3mc$ with $a=2.839(4)$ and $c=20.36(3)$ Å. The oxygen packing in this structure is ABCAACBA, and there are four CoO_2 sheets per unit cell. The Li^+ and Na^+ ions are not mixed, but are found in separate planes between the CoO_2 sheets: the Li^+ ions are in octahedral coordination with oxygen, while the Na^+ ions are in trigonal prisms. The Na^+ ion has two trigonal

*Corresponding author.
E-mail address: j.w.g.bos@ed.ac.uk (J.W.G. Bos).

0022-4596/$ - see front matter Published by Elsevier Inc.
doi:10.1016/j.jssc.2007.09.002

prismatic sites available, analogous to the 2-layer Na_xCoO_2 phase [8]. More recently, the thermoelectric properties of this phase at composition $Li_{0.48}Na_{0.35}CoO_2$ were reported [13]. At room temperature, a thermopower of 180 μV/K and resistivity of 20 mΩ cm were observed. The reported thermal conductivity is $2\,W\,m^{-1}\,K^{-1}$ (cf. Bi_2Te_3 has $3\,W\,m^{-1}\,K^{-1}$ at 300 K) [14] leading to a thermoelectric figure of merit (ZT) of 0.02 at 300 K. Improvement of ZT will depend on reduction of the resistivity. For example (keeping everything else constant), a resistivity of 1 mΩ cm would lead to a ZT~0.4 at 300 K. Given the wide variety of electronic states observed in A_xCoO_2 (A = Li, Na) and the potential of $Li_{0.48}Na_{0.35}CoO_2$ as a thermoelectric, it is of much interest to study the structures and physical properties of $Li_xNa_yCoO_2$, where x and y are varied by intercalation and deintercalation.

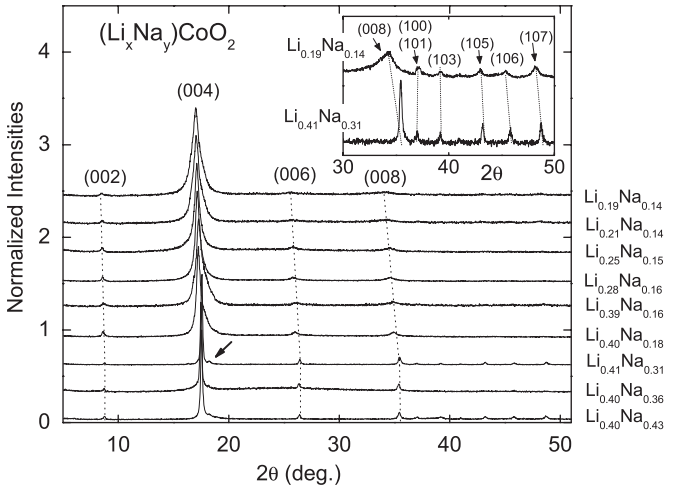

Fig. 1. Normalized Powder X-ray diffraction patterns for all studied $Li_xNa_yCoO_2$ samples. The inset contains a close up of the high angle region for the thermodynamic and most deintercalated phases. The dotted lines in the main panel are a guide to the eye.

2. Experimental

Polycrystalline $Li_xNa_yCoO_2$ with nominal $x = 0.47$ and $y = 0.44$ was prepared by standard solid state chemistry methods. Stoichiometric amounts of Na_2CO_3 (99.995%, dried at 120 °C), Li_2CO_3 (99.997%) and Co_3O_4 (99.995%, dried at 450 °C) were intimately mixed using mortar and pestle, and pressed into pellets of approximately 2 g each. These were heated at 900 °C for 12 h under a flow of oxygen in a pre-heated furnace. The samples were quenched by removing the boat from the tube furnace and placing the pellets on a thick metal plate. This process was repeated once, and finally the sample was annealed under O_2 flow at 300 °C overnight This resulted in an almost phase pure sample of $Li_xNa_yCoO_2$. From ICP-AES analysis (Inductively coupled plasma atomic emission spectroscopy), the composition of the resulting compound was found to be $Li_{0.41}Na_{0.31}CoO_2$. A trace of a Li-rich $Li_xNa_yCoO_2$ phase was found to be present (labelled with an arrow in Fig. 1).

Deintercalation of Na and Li was done via a chemical route. Finely ground powder and small bars of the thermodynamically stable phase (~$1 \times 1 \times 10\,mm^3$) were deintercalated using solutions of Br_2 and I_2 in acetonitrile (solutions of concentrations 40 × Br, 20 × Br and 10 × I of the molar excess of the total amount the Na and Li present were used). In the case of the powders 1 g in 20 ml acetonitrile were used, and the solution was stirred vigorously with a magnetic stirrer. In case of the bars about 5 bars and 5 ml acetonitrile were used without stirring. An overview of the deintercalation conditions is given in Table 1. Na intercalation was performed as follows: Na metal (0.3 g) and dry tetrahydrofuran (40 ml) were placed in a $25 \times 150\,mm^2$ pyrex screw-capped tube and heated by placing the lower 3 cm in an oil bath maintained at 95 °C. After 30 min, benzophenone (2.0 g) was added (to make an Na-benzophenone complex that is

Table 1
Compositions determined by ICP-AES, Curie constants (C), experimental (μ_{eff}) and calculated ($\mu^2_{calc} = (1-x-y)^*\ \mu^2Co^{4+}$ [$S = 1/2$]) effective moments, Weiss temperatures (θ_w), temperature independent contributions to the susceptibility (χ_0) and lattice constants for $Li_xNa_yCoO_2$

			Li_x (–)	Na_y (–)	C emu/mol Co Oe K)	μ_{eff} (μ_B/Co)	μ_{calc}	θ (K)	χ_0 (emu/mol Co Oe)	a-axis (Å)	c-axis (Å)
As prepared	–	–	0.41	0.31	0.132(5)	1.03	0.93	−85(2)	0	2.8266(3)	20.265(2)
2 × Na	Powder	4d	0.40	0.43	0.178(5)	1.19	0.71	−29(2)	0	2.8264(4)	20.305(4)
	Bar	4d	0.40	0.36	–			–	–	–	20.27(1)
10 × I	Powder	10d	0.39	0.16	0.088(5)	0.84	1.16	−30(2)	0.00023	2.827(6)	20.48(1)
	Bar	5d	0.40	0.18	–			–	–	–	20.40(1)
20 × Br	Powder	10d	0.19	0.14	0.024(5)	0.44	1.42	32(5)	0.00045	2.816(5)	20.77(1)
	Bar	5d	0.28	0.16	–			–	–	–	20.58(1)
40 × Br	Powder	10d	0.21	0.14	0.018(5)	0.38	1.40	48(5)	0.00046	2.819(4)	20.70(1)
	Bar	5d	0.25	0.15	–			–	–	–	20.70(1)

The lattice constants were obtained from the positions of the (00l) and (10l) reflections. (where standard deviations are not given they are 1 in the last decimal).

stable in THF). After the solution turned blue, powdered $Li_xNa_yCoO_2$ (1.0 g) and 2–3 bars contained in a Pasteur pipette (with a hole in its side to improve the flow) were added. The tube was again placed in the oil bath and the mixture heated for four days under magnetic stirring. After cooling to room temperature ethanol (20 ml) was added to quench the benzophenone ketyl radical anion and any unreacted sodium metal. The ethanol was decanted after 15 min, and the bars and powder was washed three times in dichloromethane (20 ml). Finally, the bars and powder were dried and stored in a desiccator.

Powder X-ray diffraction (PXRD) patterns were collected using a Bruker D8 Focus diffractometer with Cu K_α radiation fitted with a scintillation counter and a graphite diffracted beam monochromator. Lattice constants for the as-prepared sample were obtained from LeBail fits using the JANA2000 program [15]. The temperature and field dependence of the magnetic susceptibilities were measured using a Quantum Design Physical Properties Measurements System (PPMS) fitted with ACMS inset. Thermopower data were collected using an MMR technologies SB100 Seebeck measurement system. Rectangular bars (app. $1 \times 1 \times 5\,mm^2$) were mounted on a sample holder using silver paint. Electrical resistivities were measured using the resistance option of the PPMS; sample resistances were all within the acceptable measurement range. Contacts were made using platinum wire and silver paint in a standard four-point geometry. The bars were sanded down before applying the contacts.

3. Results

3.1. Composition and structure

The ICP–AES determined compositions of the studied materials are given in Table 1. The composition of the as-prepared sample is $Li_{0.41}Na_{0.31}CoO_2$ (uncertainty in Na and Li contents are approximately ± 0.01). This corresponds to a loss of 0.06 Li and 0.13 Na per formula unit from the nominal composition during synthesis. Deintercalation with $40\times$ and $20\times$ Br results in samples with nearly identical compositions. For the powder samples the compositions are $Li_{0.20}Na_{0.14}CoO_2$. For the bars, the Li content is slightly higher, at $Li_{0.25}Na_{0.15}CoO_2$. Iodine selectively deintercalates Na, and gives materials of composition $Li_{0.39}Na_{0.16}CoO_2$ for the powders, and $Li_{0.40}Na_{0.18}CoO_2$ for the bars. Note that the Na content is identical to that obtained using bromine. Sodium intercalation resulted in a powder sample with $Li_{0.40}Na_{0.43}CoO_2$, and bars with composition $Li_{0.40}Na_{0.36}CoO_2$. The samples are assumed to be oxygen stoichiometric as the starting material was annealed under an oxygen flow and chemical intercalation/deintercalation should not affect the oxygen content (as for the pure Na and Li phases [14]).

The PXRD patterns of all studied samples are shown in Fig. 1. The pattern of the thermodynamically stable phase is in good agreement with the literature [12,13]. The refined lattice constants are $a = 2.8266(3)$ Å and $c = 20.265(2)$ Å. Deintercalation strongly affects the PXRD peak shapes (Fig. 1), making Rietveld fitting of the diffraction data problematic. For this reason, the lattice constants were directly obtained from the peak positions of the (00*l*) and (10*l*) reflections. Determination of the *a*-axis is only given for compositions where at least three (10*l*) reflections were visible in the diffraction pattern (see inset to Fig. 1). From Table 1 and Fig. 2a, it can be seen that deintercalation results in a systematic increase in the *c*-parameter. This reflects the increased coulomb repulsion between the CoO_2 layers upon deintercalation that is also observed for the A_xCoO_2 (A = Li, Na) series [6,8–10]. The Na intercalated samples have very similar *c*-parameters, not continuing the trend that is seen in the deintercalated samples (Fig. 2a). Furthermore, the Na intercalated powder sample is the only non-thermodynamically stable sample that has sharp PXRD reflections. The trend for the *a*-axis is masked by the relatively large standard deviations (Table 1). For the related A_xCoO_2 (A = Li, Na) series, a shortening of the *a*-axis with x is observed. The full-width half-maximum (FWHM) of the (004) reflections of the studied materials are shown in Fig. 2b. This reveals that the extraction of Na

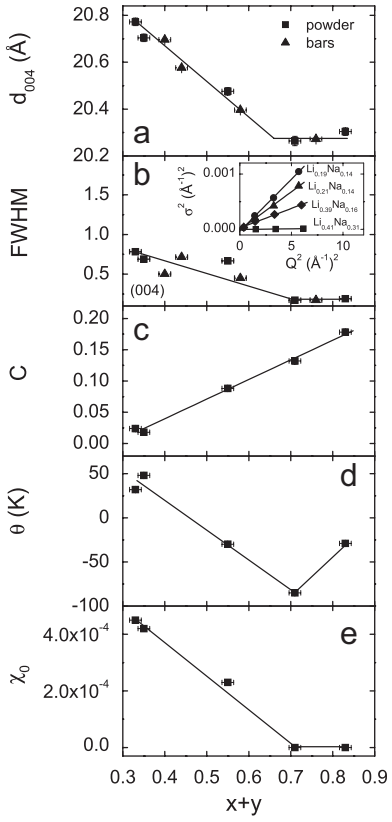

Fig. 2. The dependence of (a) the crystallographic *c*-axis (Å), (b) the full-width at half-maximum (FWHM) of the (004) reflection, the inset shows the peak width variance for the (00*l*) reflections for selected $Li_xNa_yCoO_2$ samples. (solid lines are linear fits), (c) the Curie constants (C in emu/mol Co Oe K), (d) the Weiss temperatures (θ_w in K) and (e) χ_0 (χ_0 in emu/mol Co Oe) on total alkali ion content ($x+y$) for $Li_xNa_yCoO_2$.

and Li from the parent phase leads to an increasingly poorer structural coherence. The broadening of the (00*l*) reflections can be deconvoluted into contributions due to particle size and microstrain using a Williamson-Hall plot (inset to Fig. 2b) [16]. The size and microstrain contributions to the peak widths are described by:

$$\sigma^2(Q_i) = \frac{\pi^2}{2\ln 2}\frac{1}{L^2} + \langle e^2\rangle Q_i^2, \quad (1)$$

where σ^2 is the variance of the peak width ($\sigma^2 = \mathrm{FWHM}^2/8\ln 2$), Q is the wave vector transfer, L is the mean dimension of the particles and $\langle e^2\rangle$ is the variance of the stress distribution. The FWHM were corrected for instrumental broadening effects using an Al_2O_3 standard. The inset to Fig. 2b shows that the peak variance approaches zero when Q^2 goes to zero, revealing that the effects of particle size broadening are negligible. The microstrain contribution to the peak width (the slopes in the inset of Fig. 2b), on the other hand, increases significantly upon chemical deintercalation. The broadening of the (00*l*) reflections indicates that the crystallinity is reduced during the chemical deintercalation process. The analysis described above shows that this is due to microstrain broadening (probably related to remnant stresses in layer stacking) and not due to smaller particle sizes. It is not clear why strain-induced reduced crystallinity occurs for deintercalated $Li_xNa_yCoO_2$ but not for A_xCoO_2 (A = Na, Li), in spite of the similar synthesis procedures. Note that the reduced crystallinity does not imply that Na and Li are mixing upon deintercalation: in all PXRD patterns the (002) reflection is present. This reflection can only be present if the Li and Na layers remain distinct. The fact that it is visible for all studied samples indicates that the layered arrangement of Na/Li remains intact throughout the series. The structure of the "as made" material $Li_{0.41}Na_{0.31}CoO_2$ has been studied previously, and, as expected from the great size difference between Li^+ and Na^+, these ions are found in distinctly different layers in the compound [12]. In our deintercalation experiments, alkali ions are removed from the layers of the "as made" material and there is no driving force for removing an ion from one layer and reinserting it into a different layer. Thus the Li and Na layers will not mix on deintercalation. In our intercalation experiments, only Na^+ was added to the "as made" compound. This ion is too big to go into the Li^+ layer so, in the intercalation experiments as well, mixing within the alkali layers is also highly improbable. These considerations are in agreement with our observations.

3.2. Magnetic properties

The temperature dependences of the inverse magnetic susceptibilities, $1/(\chi(T)-\chi_0)$, for the powder samples are given in Fig. 3a, b. χ_0 was obtained by fitting the measured magnetic susceptibility to the Curie Weiss law $\chi(T) = C/(T-\theta_w)+\chi_0$ from 100 to 250 K. The insets to Fig. 3 show the measured susceptibilities without the χ_0 subtraction.

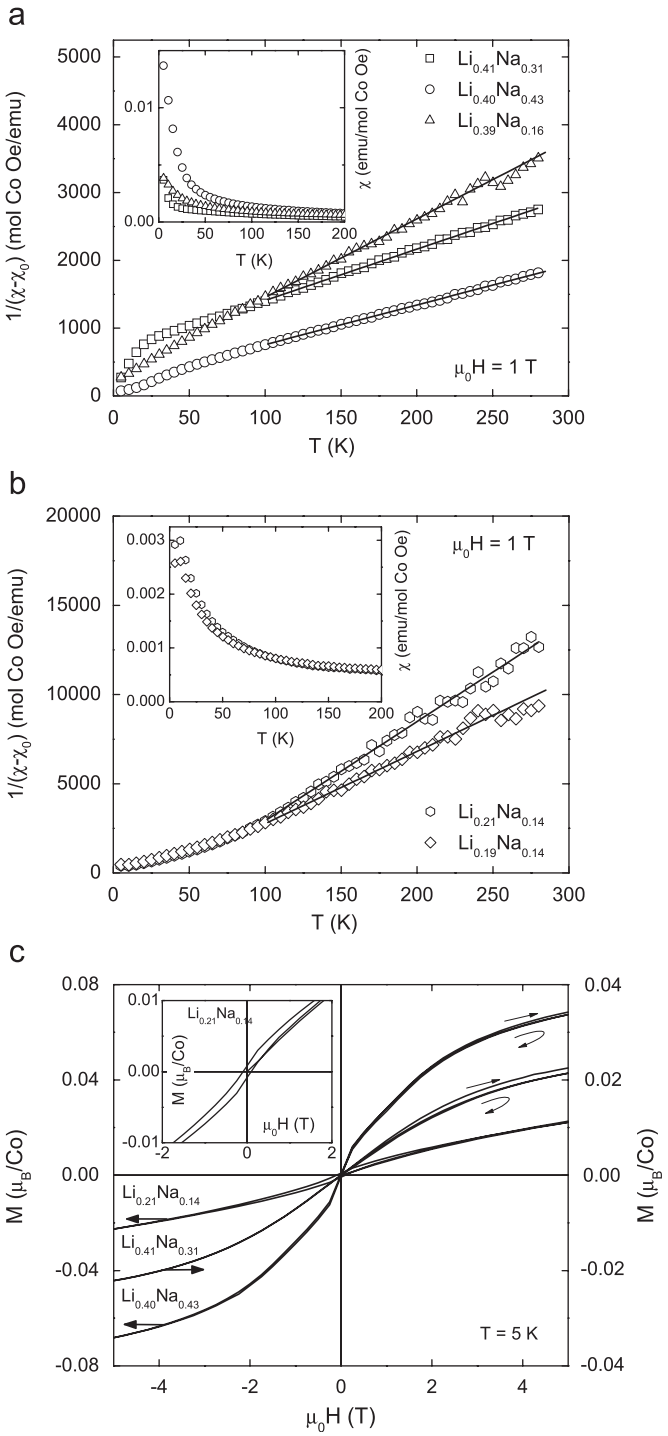

Fig. 3. (a, b) The temperature dependences of the inverse magnetic susceptibilities $[1/(\chi-\chi_0)]$ for selected $Li_xNa_yCoO_2$ samples. Solid lines are fits to the Curie Weiss law. The insets show the temperature dependences of the measured magnetic susceptibilities without the subtraction of χ_0. (c) $M(H)$ loops for selected $Li_xNa_yCoO_2$ compositions.

The obtained Curie constants (C), Weiss temperatures (θ_w) and temperature-independent contributions to the susceptibility (χ_0) are given in Table 1 and Fig. 2c–e. The solid lines in Fig. 3 are linear fits. The downturn of the inverse susceptibility below 50 K in Fig. 3a suggests the onset of a

magnetic ordering transition, with a ferromagnetic component, in spite of the fact that the negative Weiss temperature indicates the presence of dominantly antiferromagnetic interactions. This type of behaviour is commonly observed in systems such as canted antiferromagnets, where the ordering is basically antiferromagnetic in character but due to small deviations of the spins from antiparallel alignment in the ordered state, some ferromagnetic component is observed. The magnetic transition is most pronounced for the as-prepared sample $Li_{0.41}Na_{0.31}CoO_2$ but, as revealed by the inset, also occurs for the Na-intercalated sample $Li_{0.40}Na_{0.43}CoO_2$. The sharp upturn in the magnetic susceptibility disappears for the samples treated with iodine and bromine (Fig. 3a, b). For $Li_{0.40}Na_{0.16}CoO_2$, the inverse susceptibility remains almost linear down to 5 K. A small downturn at low temperatures remains visible. For the samples treated with bromine the Weiss temperatures are positive and within error identical (Table 1 and Fig. 2d). Both show an antiferromagnetic-like transition at 10 K (Fig. 3b). This kind of behaviour is frequently observed in layered systems where in-plane correlations are ferromagnetic in character and inter-plane interactions are antiferromagnetic in character. The as-prepared sample $Li_{0.41}Na_{0.31}CoO_2$ has an effective moment of $1.0\,\mu_B$/Co, close to the spin-only moment expected for the low spin mixture of 0.28 Co^{4+} ($S=1/2$) + 0.72 Co^{3+} ($S=0$), $0.9\,\mu_B$/Co, that would result for this composition, though we have no data to directly measure the Co spin states. The data show that the Curie constant increases with increasing $x+y$ (Fig. 2c and Table 1). This trend suggests that the system is one in which high spin or intermediate spin Co is introduced as the formal Co valence approaches Co^{3+}. This is similar to what is observed in the 3-layer Na_xCoO_2 series [9]. The bottom three panels of Fig. 2 summarize the magnetic characteristics of the system. The temperature-independent contribution (χ_0) to the susceptibility changes from ~0 to $+4.5\times10^{-4}$ emu/mol Co Oe (Table 1 and Fig. 2e) with decreasing $x+y$. This indicates the presence of a significant Pauli paramagnetic contribution to the susceptibility that increases with increasing formal oxidation of Co. This observation, and the decreasing magnitude of the curie constant with increasing Co oxidation indicate the strong tendency toward charge delocalization on oxidation of Co. This trend is in agreement with resistivity measurements (Fig. 4) that show metallic-like temperature dependence for these compositions ($x+y<0.58$). The field dependences of the $T=5$ K magnetizations of selected samples are shown in Fig. 3c. The as-prepared $Li_{0.41}Na_{0.31}CoO_2$ and Na-intercalated $Li_{0.40}Na_{0.43}CoO_2$ samples show no magnetic hysteresis. The bromine deintercalated sample $Li_{0.21}Na_{0.14}CoO_2$ showed a small magnetic hysteresis, consistent with the positive Weiss temperature discussed above. The small magnitudes of the magnetizations suggest that no long range purely ferromagnetic ordering occurs in any of the samples.

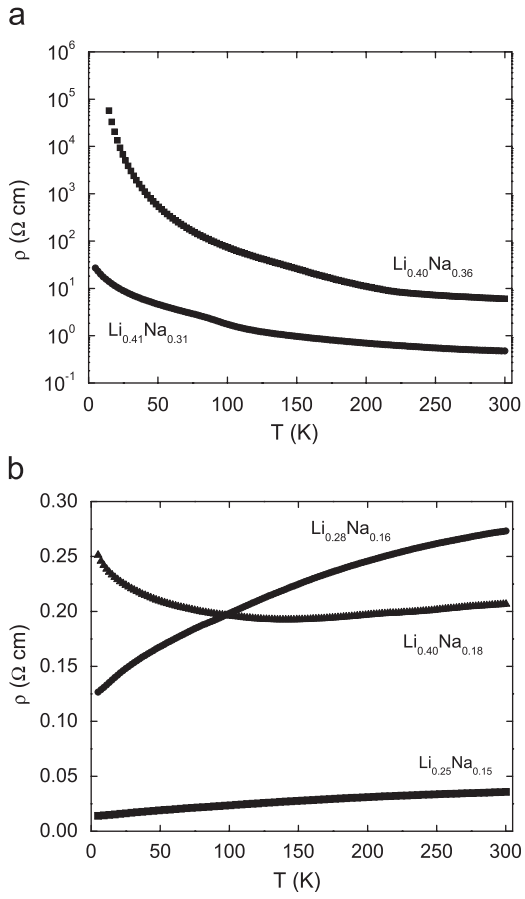

Fig. 4. Temperature dependences of the electrical resistivities (ρ) measured on polycrystalline samples for selected $Li_xNa_yCoO_2$ compositions.

3.3. Electrical resistivity and thermopower

The temperature dependences of the resistivities are given in Fig. 4. Because the data are taken on polycrystalline samples, they can be interpreted only qualitatively. Thermodynamically stable $Li_{0.41}Na_{0.31}CoO_2$ and intercalated $Li_{0.40}Na_{0.36}CoO_2$ are both semiconducting, with resistivities of 0.5 and 6 Ω cm at 300 K, respectively (Fig. 4a). The temperature dependence could not be fitted with thermally activated or variable range hopping behaviour. Deintercalation results in a transition to metallic-like behaviour (Fig. 4b), though the measured resistivities remain high, 40–270 mΩ cm at 300 K. The resistivity of the iodine deintercalated sample $Li_{0.40}Na_{0.18}CoO_2$ shows a transition from a metallic to a semiconducting temperature dependence around 125 K. The residual resistivity ratios for the bromine deintercalated samples are approximately 2, combined with the magnitude of the metallic-like resistivities, this suggests that grain boundary effects strongly influence the measured resistivity.

The thermopowers of the $Li_xNa_yCoO_2$ samples are given in Fig. 5. The thermodynamically stable phase proved difficult to measure reproducibly, possibly due to chemical changes during the measurement. The data shown in Fig. 5a are the average of 3 measurements; the relatively

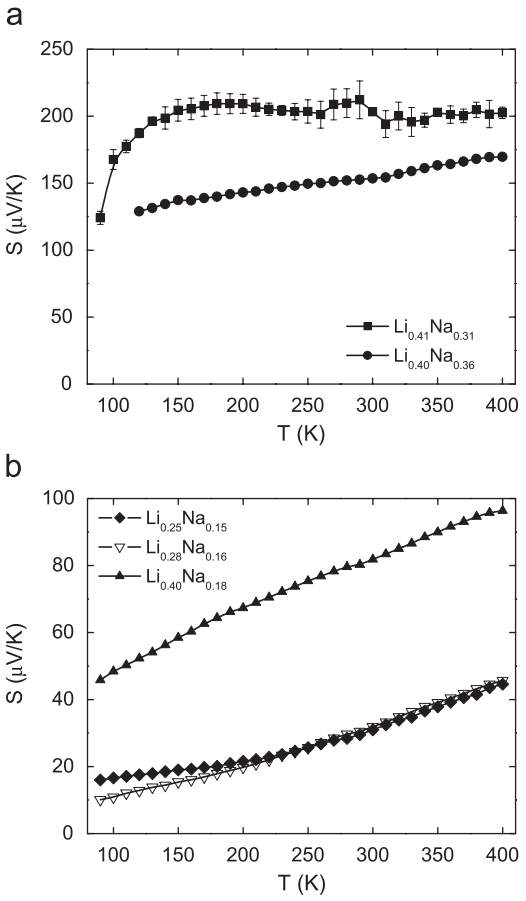

Fig. 5. Temperature dependences of the thermopowers (S) for selected $Li_xNa_yCoO_2$ compositions.

large error bars reveal the deviations among the measurements. The measured thermopower increases to a maximum value just above 200 μV/K. No reproducibility problems were observed for the other samples; the error bars are much smaller than the symbols. The thermopowers of the non-thermodynamically stable samples all have linear temperature dependences that are characteristic of metals or degenerate semiconductors. The room temperature values vary between 30 μV/K ($Li_{0.25}Na_{0.16}CoO_2$) and 150 μV/K ($Li_{0.41}Na_{0.36}CoO_2$). The thermopowers of the bromine deintercalated samples (Fig. 5b) are nearly identical. This suggests that the difference in resistivities (Fig. 4b) for these two samples are due to grain boundary or other microstructure effects. This is in agreement with the fact that the residual resistivity ratios are identical. The resulting thermoelectric power factors ($PF = S^2/\rho$) are low ($<0.1\,\mu W/K^2\,cm$), largely due to the high electrical resistivities.

4. Discussion

The layered $Li_xNa_yCoO_2$ materials have been prepared by solid state reaction and chemical deintercalation/intercalation reactions. The Na and Li ions are arranged in alternating layers sandwiched between CoO_2 sheets. The alkali ion content ($x+y$) was varied between 0.33 and 0.84, corresponding to formal cobalt valences of +3.76 and +3.17. The physical properties of the present series and A_xCoO_2 (A = Li or Na) show many similarities: for example, a transition from insulating to metallic behaviour with decreasing x ($x+y$) is observed. In the current case the transition falls between $x+y=0.72$ and $x+y=0.58$; the exact composition has not been determined. The linear temperature dependence of the thermopower for a wide range of x was previously observed for Li_xCoO_2 [10]. The main difference in the Li–Na phase is the loss of structural coherence: both A_xCoO_2 (A = Li, Na) series can be chemically intercalated and deintercalated without any loss in structural integrity. Detailed X-ray and neutron powder diffraction studies have been reported for the 3-layer Li [6] and 2- and 3-layer [8,9] Na series. The studies on Na_xCoO_2 reveal clear correlations between the shapes of the CoO_6 octahedra, the Na-ion positions and the electronic phase diagram. This shows the importance of the coupling of the structural and electronic degrees of freedom in these materials. The loss of structural coherence in the $Li_xNa_yCoO_2$ series is expected to have profound consequences for the electronic properties. The thermopowers, which are less sensitive to microstructure effects, are characteristic of metals or degenerate semiconductors, and fall between 30 and 80 μV/K for the deintercalated samples at RT. For comparison, single crystalline $Na_{0.7}CoO_2$ is reported with a thermopower of 90 μV/K and an electrical resistivity of 0.2 mΩ cm, leading to a thermoelectric power factor of 50 $\mu W/K^2\,cm$ [3]. The low thermoelectric power factors ($\leqslant 0.1\,\mu W/K^2\,cm$) in the current series can therefore be attributed mainly to the high electrical resistivities. The semiconducting samples have higher thermopowers but this is offset by the much higher resistivities. We were not able to reproduce the result from Ref. [13] ($PF = 1.6\,\mu W/K^2\,cm$). The future development of a preparation route where the structural integrity remains intact may lead to materials suitable for thermoelectric applications.

Acknowledgments

This research was supported by the Air Force Office of Scientific Research, Grant FA9550-06-1-0530. JWGB acknowledges support from the Royal Society of Edinburgh.

References

[1] K. Mizushima, P.C. Jones, P.J. Wiseman, et al., Materials Research Bulletin 15 (1980) 783.
[2] M.L. Foo, Y.Y. Wang, S. Watauchi, et al., Physical Review Letters 92 (2004) 247001.
[3] I. Terasaki, Y. Sasago, K. Uchinokura, Physical Review B 56 (1997) 12685.
[4] M. Lee, L. Viciu, L. Li, et al., Nature Materials 5 (2006) 537.
[5] K. Takada, H. Sakurai, E. Takayama-Muromachi, et al., Nature 422 (2003) 53.

[6] J.N. Reimers, J.R. Dahn, Journal of the Electrochemical Society 139 (1992) 2091.
[7] C. Fouassie, G. Matejka, J.M. Reau, et al., Journal of Solid State Chemistry 6 (1973) 532.
[8] Q. Huang, M.L. Foo, R.A. Pascal, et al., Physical Review B 70 (2004) 184110.
[9] L. Viciu, J.W.G. Bos, H.W. Zandbergen, et al., Physical Review B 73 (2006) 174104.
[10] M. Menetrier, I. Saadoune, S. Levasseur, et al., Journal of Materials Chemistry 9 (1999) 1135.
[11] S. Park, Y. Lee, T. Vogt, arXiv:cond-mat/0407778 (2004).
[12] R.J. Balsys, R.L. Davis, Solid State Ionics 69 (1994) 69.
[13] Z. Ren, J. Shen, S. Jiang, et al., Journal of Physics-Condensed Matter 18 (2006) L379.
[14] D.R. Lide, CRC Handbook of Chemistry and Physics, 87th ed., Taylor and Francis, Boca Raton, FL, 2007.
[15] V. Petricek, M. Dusek, L. Palatinus, Institute of Physics, Praha, Czech Republic, 2000.
[16] G.K. Williamson, W.H. Hall, Acta Metall. 1 (1953) 22.